

PLASTICITY CORRECTION FACTORS FOR BUCKLING OF FLAT RECTANGULAR GLARE PLATES LOADED IN COMPRESSION OR SHEAR

T. C. Wittenberg

Faculty of Aerospace Engineering, Delft University of Technology
Kluyverweg 3, 2629 HS Delft, The Netherlands

A. de Jonge

Fokker Aerostructures B.V.
PO Box 1, 3350 AA Papendrecht, The Netherlands

Keywords: *Glare, plastic buckling, J2-deformation/flow theory, flat plates*

Abstract

Glare is a Fibre Metal Laminate that consists of alternate aluminium sheets and glass fibre pre-impregnated layers. For higher stress levels, the aluminium sheets will become plastic. For relatively thick Glare plates this also implies that buckling will take place non-elastically.

In this paper, a methodology is proposed to calculate plasticity reduction factors for flat Glare plates either loaded in compression or shear. This method uses J2-deformation theory to describe the plastic behaviour of the metal laminae in combination with a Ramberg-Osgood stress-strain relation.

A number of non-linear FEM calculations is made on imperfect plates using J2-flow theory for the metal laminae. The effect of the imperfection on the buckling load is studied and a comparison is made between the reduction factor calculated both ways.

Possible set-ups for an experimental verification of the theory are also discussed.

Notation

ε_{ij} = tensorial strains
 σ_{ij} = tensorial stresses
 τ = engineering shear stress = σ_{12}
 γ = engineering shear strain = $2\varepsilon_{12}$
 E = Young's modulus
 E_s = secant modulus

E_t = tangent modulus
 G = shear modulus
 G_s = shear secant modulus
 t = plate thickness
 a = plate length
 b = plate width
 η_c = plasticity correction factor for compression
 η_s = plasticity correction factor for shear
 ν = elastic Poisson's ratio
 ν_s = elasto-plastic Poisson's ratio
 σ_{cr} = critical compressive buckling stress
 σ_y = 0.2% yield stress of aluminium
 σ_M = Von Mises stress
 $[= \sqrt{(\sigma_{11}^2 + \sigma_{22}^2 - \sigma_{11}\sigma_{22} + 3\sigma_{12}^2)}]$
 τ_{cr} = critical shear buckling stress
 $[A_{ij}]$ = laminate in-plane stiffness matrix
 $[D_{ij}]$ = laminate bending stiffness matrix
 $[C_{ij}]$ = flexibility matrix of metal sheet
 $[S_{ij}]$ = stiffness matrix of metal sheet

1 Introduction

Glare is a fibre metal laminate that possesses excellent fatigue characteristic combined with a relatively low density. For these reasons, amongst others, it is a candidate material for fuselage skins in future generation Ultra-High Capacity Aircraft (UHCA) [1]. For aircraft of this size, the skin will be relatively thick, so that

skin buckling is prone to happen in the plastic region. It can be shown that Glare is more efficient (in terms of weight) than aluminium in preventing elastic plate buckling [2].

In the case of plastic buckling, it is common design practice to apply a “plasticity correction factor” to the critical buckling load calculated with elastic material properties. For pure aluminium such factors exist for compression, and have been validated by experiments performed in the nineteen-forties and fifties by the NACA [3]. The correction factor η is defined as the ratio of the plastic buckling load and the buckling load based on pure elastic behaviour.

For compression loading, the following plasticity correction factor is generally used [4]:

$$\eta_c = \frac{E_s}{2E} \left(\frac{1-\nu^2}{1-\nu_s^2} \right) \left(1 + \sqrt{\frac{1}{4} + \frac{3}{4} \frac{E_t}{E_s}} \right) \quad (1)$$

For inelastic shear buckling, Gerard [5] suggested the use of the shear secant modulus, or

$$\eta_s = \frac{G_s}{G} \quad (2)$$

This approach was shown to be in good agreement with test results of aluminium plates.

The plasticity correction factor given by Eq. (1) for an aluminium plate loaded in compression can be derived analytically using the so-called J2-deformation theory of plasticity (see, for example, Ref. [6]). Predictions based on the more common J2-flow theory of plasticity lead to unrealistically high predictions for the plastic bifurcation-buckling load. In the past, this has led to a lot of discussion because there is no sound physical basis for J2-deformation theory, which is essentially a non-linear elastic theory, whereas there is a good physical justification for J2-flow theory. In the literature, this has led to a debate as to the cause of this paradox. Some authors argued that small initial imperfections on the geometry would lower the buckling load predicted by J2-flow theory. Other people

proposed an alternative flow theory of plasticity, which can develop a corner on the yield surface. This theory leads to the same predictions as deformation theory for bifurcation problems [7]. The question whether the buckling value is due to (imperfections on) the geometry or due to the material, remains up till now unresolved. However, in his famous paper [7], Hutchinson, concluded that for engineering purposes J2-deformation theory should be the preferred plasticity theory for bifurcation problems.

In the present paper a methodology is presented to calculate the plasticity correction factors for buckling of flat rectangular Glare plates subjected to compressive or shearing loads. Results are presented for two types of Glare plates and three values of the Ramberg-Osgood strain hardening parameter. Comparisons will also be made with FEM calculations of imperfect plates for which J2-flow theory is used for the aluminium layers. In these analyses the influence of the size of the imperfection on the plastic buckling load is investigated.

For both compression and shear loading, buckling analysis is performed using the same general partial differential equation that governs equilibrium of the plate in the buckled state. This equation involves elements of the flexural stiffness matrix of the plate, which are calculated by using elasto-plastic moduli of the aluminium layers. The plasticity reduction factors do not depend on the size of the specimens, and therefore the method is suitable to generate design curves that depict the plasticity correction factor versus the buckling stress, as commonly used in the aircraft industry.

Although not impossible, experiments to determine the plasticity reduction factors are very complicated because of the difficulty to implement totally simply supported or fully clamped boundary conditions. It will therefore not come as a surprise that the proposed method has not been experimentally verified yet. In this paper possible set-ups for tests will be discussed.

2 The Glare material

Glare consists of alternate aluminium sheets and unidirectional high-strength glass fibre layers pre-impregnated with adhesive (see Ref. [1]). The most common type of aluminium applied in Glare is 2024-T3 alloy. Each glass prepreg layer is composed of a certain number of unidirectional (UD) plies, which are stacked either unidirectionally, or, most commonly, in a cross-ply arrangement. The number, orientations, and the stacking sequence of the UD plies in the prepreg layer depend on the Glare *grade*. For example, a Glare 2 has two UD plies in a single prepreg layer with the same 0-degree orientation, while a Glare 3 has two perpendicular UD plies. For a Glare 3 with an even number of glass layers, the plies are placed such that the overall laminate is symmetric. The thickness of each UD ply is 0.125 mm, so that the prepreg layers of both Glare 2 and 3 have a total thickness of 0.25 mm. Note that the outer layers in Glare are always aluminium, so that the number of glass fibre layers is always one less.

A general Glare configuration is represented as:

$$\text{Glare } \textit{grade} - N_{al} / N_{gl} - t_{al}$$

where

grade = glare grade (currently 1, 2, 3, 4 or 5)

N_{al} = number of aluminium layers

N_{gl} = number of glass fibre layers

t_{al} = aluminium sheet thickness

Two different Glare 3 types are considered for the compression and shear case. These are given in Table 1 and Table 2, respectively. The aluminium and glass layer properties are given in Table 3, and were taken from the MIL

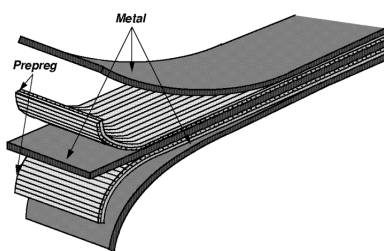


Fig. 1. A typical Glare 3-3/2 laminate.

Table 1. Glare type used for the compression case.

Name	Glare 3-7/6-0.4
Total thickness	4.3 mm
Aluminium	2024-T3

Table 2. Glare type used for the shear case.

Name	Glare 3-5/4-0.4
Total thickness	3.0 mm
Aluminium	2024-T3

Table 3: Material properties used

	Prepreg (0/90)	2024-T3	
G	4750	27218	MPa
ν	0.144	0.33	
E_{11}	30753	72400	MPa
E_{22}	30753	72400	MPa
σ_y	-	290	MPa

handbooks [8, 9]. Note that in our analysis here, the prepreg properties of a 0/90 degree combination are considered as one layer. Furthermore, the anisotropy of the rolled aluminium sheet is not taken into account.

3 Calculation method

For Glare plates loaded beyond the yield strength, the aluminium layers become plastic, but the glass layers remain elastic. The behaviour of a Glare plate loaded in the plastic region therefore essentially differs from a monolithic aluminium plate.

The proposed calculation method employs classical laminate theory (CLT) to calculate the in-plane stiffnesses, A_{ij} , and the out-of-plane bending rigidities, D_{ij} (according to the definition in Ref. [10]). Elasto-plastic moduli are used for the aluminium layers in combination with a Ramberg-Osgood (RO) fit for the stress-strain behaviour.

3.1 Buckling analysis

For compression, the critical buckling stress, σ_{cr} , for a simply supported, orthotropic, long plate is calculated with the following formula [2]:

$$\sigma_{cr} = \frac{2\pi^2}{tb^2} \left[\sqrt{D_{11}D_{22}} + D_{12} + 2D_{33} \right] \quad (3)$$

Note that the coefficients D_{ij} depend on the stress; suffix 1 refers to the long axes.

Although no closed-form solution exists for shear buckling, the following exact solution can be derived for an infinitely long, orthotropic plate [10]

$$\tau_{cr} = 4\beta \frac{\sqrt[4]{D_{11}D_{22}^3}}{tb^2} \quad (4)$$

which is only valid if the condition

$$\theta = \sqrt{D_{11}D_{22}/(D_{12} + 2D_{33})^2} \geq 1 \quad (5)$$

is satisfied. The coefficient β appearing in Eq. (4) is given in Ref. [10] in tabulated form. For the Glare type used in this paper (Glare 3-5/4-0.4), it can be shown that $1 \leq \theta \leq 3$, in which range the tabulated data can be fitted with the following curve:

$$\beta = 0.76\theta^2 - 4.65\theta + 17.06 \quad (6)$$

3.2 Ramberg-Osgood relations

The elasto-plastic stress-strain behaviour of an aluminium layer will be described by a Ramberg-Osgood representation of the following type:

$$\varepsilon = \frac{\sigma_M}{E} + \alpha \frac{\sigma_y}{E} \left(\frac{\sigma_M}{\sigma_y} \right)^n \quad (7)$$

$$\alpha = \frac{0.002E}{\sigma_y} \quad (8)$$

In fact, the effective strain, ε , is not explicitly used. Instead, the secant modulus, E_s , and the tangent modulus, E_t are used:

$$E_s = \frac{E}{1 + \alpha \left(\frac{\sigma_M}{\sigma_y} \right)^{n-1}} \quad (9)$$

$$E_t = \frac{E}{1 + \alpha n \left(\frac{\sigma_M}{\sigma_y} \right)^{n-1}} \quad (10)$$

For a state of pure shear, for which $\sigma_M = \tau\sqrt{3}$, the axial stress-strain curve represented by Eq. (7) can be transformed to the relation

$$\gamma = \frac{\tau}{G} + \alpha \frac{\sigma_y}{\sqrt{3}G} \left(\frac{\sqrt{3}\tau}{\sigma_y} \right)^n \quad (11)$$

which now obviously represents the shear stress-strain curve. The shear secant and tangent modulus can now conveniently be obtained from this relation, analogous to Eqs. (9) and (10).

3.3 Stiffnesses of aluminium for compression

To calculate the membrane stiffnesses, A_{ij} , of the Glare plate, J2-flow theory is employed for the (ply) stiffness moduli of the aluminium sheets. For the bending rigidities, D_{ij} , one the other hand, J2-deformation theory is used. In this way, it is guaranteed that the stresses and strains prior to bifurcation are in accordance with the well-verified flow theory, but the bifurcation load is determined from deformation theory. Note that when using J2-deformation theory for both in-plane and bending behaviour, the results change only marginally.

Essential for the behaviour of the aluminium sheets in Glare is that the loading is biaxial, even in case where the Glare plate is subjected to uniaxial compression. This makes definition of the stiffness moduli a little bit more complex. In fact, it is more appropriate to write down the components of the compliance matrix, C_{ij} . The inverse of this matrix is the stiffness matrix. The flexibility matrix for J2-deformation theory is defined as follows [11]:

$$\begin{bmatrix} \dot{\epsilon}_{11} \\ \dot{\epsilon}_{22} \\ 2\dot{\epsilon}_{12} \end{bmatrix} = \begin{bmatrix} C_{11} & C_{12} \\ C_{12} & C_{22} \\ & & C_{33} \end{bmatrix} \begin{bmatrix} \dot{\sigma}_{11} \\ \dot{\sigma}_{22} \\ \dot{\sigma}_{12} \end{bmatrix} \quad (12)$$

with

$$C_{12} = -\frac{\nu_s}{E_s} - \left(\frac{1}{E_t} - \frac{1}{E_s} \right) \left(\frac{1}{2} - \frac{3}{4} \frac{\sigma_{11}\sigma_{22}}{\sigma_M^2} \right)$$

$$C_{22} = \frac{1}{E_s} + \left(\frac{1}{E_t} - \frac{1}{E_s} \right) \left(1 - \frac{3}{4} \frac{\sigma_{11}^2}{\sigma_M^2} \right)$$

$$C_{11} = \frac{1}{E_s} + \left(\frac{1}{E_t} - \frac{1}{E_s} \right) \left(1 - \frac{3}{4} \frac{\sigma_{22}^2}{\sigma_M^2} \right)$$

$$C_{33} = \frac{2(1+\nu_s)}{E_s} \quad (13a, b, c, d)$$

where

$$\frac{\nu_s}{E_s} = \frac{\nu}{E} + \frac{1}{2} \left[\frac{1}{E_s} - \frac{1}{E} \right] \quad (14)$$

For J2-flow theory, the same formulas can be used with the following substitutions:

$$\begin{aligned} E_s &\rightarrow E \\ \nu_s &\rightarrow \nu \end{aligned} \quad (15)$$

Note that proposed moduli are correct in the finite strain domain as well, if the strain is interpreted as the logarithmic strain and the stress as the Kirchoff stress tensor.

3.4 Stiffnesses of aluminium for shear

For this case, there is only one stress component, and, therefore, both plasticity theories predict the same pre-bifurcation path; hence, only J2-deformation theory needs to be considered. The stiffness matrix can be obtained from Ref. [12] for example, and is given here explicitly as

$$\begin{bmatrix} \dot{\sigma}_{11} \\ \dot{\sigma}_{22} \\ \dot{\sigma}_{12} \end{bmatrix} = \begin{bmatrix} S_{11} & S_{12} \\ S_{12} & S_{22} \\ & & S_{33} \end{bmatrix} \begin{bmatrix} \dot{\epsilon}_{11} \\ \dot{\epsilon}_{22} \\ 2\dot{\epsilon}_{12} \end{bmatrix} \quad (16)$$

with

$$S_{11} = S_{22} = \frac{E_s}{1-\nu_s^2}$$

$$S_{12} = \frac{\nu_s E_s}{1-\nu_s^2}$$

$$S_{33} = \frac{E_s}{2(1+\nu_s)} \left[1 - \frac{E_s/E_t - 1}{E_s/E_t - (1-2\nu_s)/3} \right]$$

(17a, b, c)

Note that the shear stress does not appear in this formula, because it is implicitly included in the secant modulus. For J2-flow theory, the stiffnesses can again be obtained using Eq. (15). However, it can be shown that the S_{33} -stiffness term is the same for flow and deformation theory, which implies that the in-plane response is equal for both theories. The buckling behaviour, on the other hand, is different, since the other stiffness terms (i.e. S_{11} , S_{22} , and S_{12}) play a role in the calculation of the bending stiffness matrix.

3.5 Solution scheme

The problem in establishing the correct buckling stress is that in Eqs. (3) and (4) the coefficients D_{ij} depend on the stress level. The equation therefore has to be solved in an iterative manner. The solution approach that is utilised is similar to the incremental approach used in most non-linear FEM-packages. Small incremental steps are taken along the stress-strain path and for each point a bifurcation check is performed. In a FEM solution, such a bifurcation would appear as a negative eigenvalue in the tangent stiffness matrix.

The following iterative solution procedure is used:

1. Choose a step size for the applied stress. (Typical stress level of a thousandth of yield stress).
2. Calculate laminate membrane stiffnesses (A-matrix) using J2-flow theory incremental moduli for metal laminae. (Note that there is no distinction between flow and deformation theory for pure shear loading.)
3. Calculate incremental strains by multiplying inverse of A-matrix with applied load vector and calculate actual strains.
4. Calculate metal layer incremental stresses from the incremental strains by means of the J2-flow theory stiffness moduli for the metal laminae and calculate actual laminae stresses.
5. Calculate D-matrix for laminate using J2-deformation theory incremental moduli.
6. Calculate buckling stress for this laminate with Eqs. (3) or (4).
7. Check whether buckling stress is higher or lower than applied stress
 - if buckling stress is lower increase load and continue at step 2,
 - else, if buckling load is higher, solution is found.

In principle, the proposed algorithm (apart from the linear buckling analysis in step 6) is valid for biaxial loading, but in this paper only results for uniaxial loading will be presented. Note that it may easily be shown that for an aluminium plate the proposed solution leads exactly to the classical reduction factor of Eq. (1) if $\nu_s = 0.5$ is taken.

3.6 Results for compression

For compression, three calculations have been made using above given solution scheme for three typical values of the RO-hardening parameter n (7.5, 10, 15). The results of these calculations are given in Fig. 2, together with a curve for solid aluminium.

At first glance, the three curves for Glare are very similar to the curves for solid aluminium. Two major differences are striking. The first influence of plasticity occurs for buckling stresses in the order of 0.5 times the aluminium yield stress. It is clear that this stress

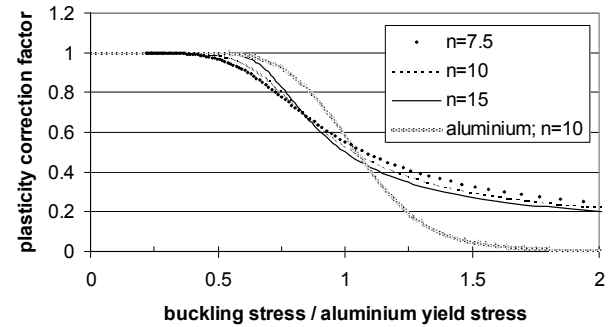


Fig. 2. Plasticity correction factor versus normalised buckling stress for compression buckling for three values of RO-parameter.

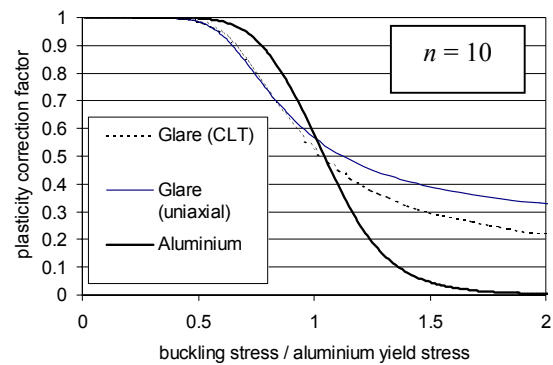


Fig. 3. Comparison of plasticity correction factor based on uniaxial stress-strain curve and analysis proposed in this paper.

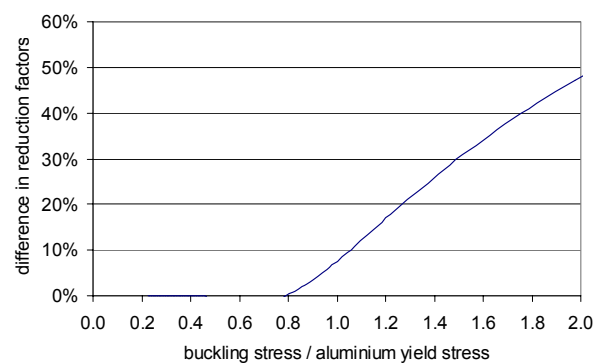


Fig. 4. Relative difference between solution based on uniaxial stress-strain curve and as proposed in this paper

is lower than for pure aluminium, because the stiffness of the glass is much lower than the stiffness of the aluminium. The actual stresses in the aluminium laminae are, therefore, higher than the average stress in the laminate. The second major difference is the behaviour for high buckling stresses. For aluminium, the

curve goes asymptotically to zero, whereas for Glare, the values remain finite. Of course, this is due to the fibres that remain elastic.

An alternative calculation was made using the classical isotropic formula for the plasticity reduction [Eq. (1)] in combination with the uniaxial stress-strain curve of Glare to determine the tangent and secant moduli. Results of this calculation are given in Fig. 3. The curve obtained with the CLT-based analysis described in this paper is below the curve obtained using the alternative solution method. The reason for this behaviour is that the membrane stiffness does not decrease as fast as the bending stiffness for a reduced stiffness of the aluminium due to plasticity. This is due to the lay-up of Glare where at the outside always aluminium layers are placed. The relative difference between the two methods is displayed in Fig. 4. For stress levels above 0.8 times yield of aluminium the difference between these methods rapidly increases. For lower stress levels, the stiff aluminium is governing and the Glare laminate is still behaving isotropically, but for higher stress levels the contribution of the Glass fibres becomes important.

It may be concluded that any simplifying model intended to describe the plasticity reduction of a fibre metal laminate over the whole range, has to contain a parameter that expresses the metal contribution to the bending stiffness.

As it is, the metal contribution to the bending stiffness is different for each Glare configuration. Curves as in Fig. 2 are therefore, in principle, only valid for one Glare configuration. In practice, however, the difference between two Glare configurations of the same grade (Glare 2, 3 or 4) is only very small, and certainly much smaller than the influence of the RO-parameter, n .

3.7 Results for shear

Similar calculations as discussed in the previous section were made for shear-loaded panels, and the results are presented in Fig. 5. The curves look very similar to the ones for compressed

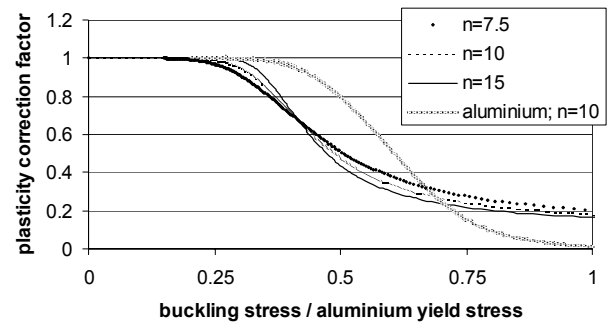


Fig. 5. Plasticity correction factor versus normalised buckling stress for shear buckling for three values of RO-parameter.

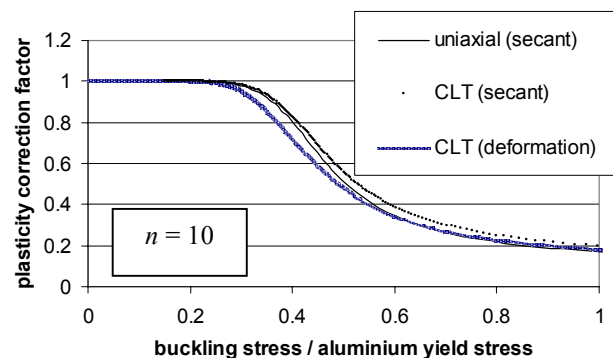


Fig. 6. Comparison of plasticity reduction factor based on “uniaxial” shear stress-strain curve and CLT-based analysis.

plates (see Fig. 2), but, looking at the pure aluminium plate, the effect of plasticity starts at lower loads. This is due to the lower value of shear yield stress—in fact, $\tau_y = \sigma_y/\sqrt{3}$ from the Von Mises relationship—so that inelastic effects are more pronounced compared to the compression case. (Note that the buckling stress is normalised with the *axial* yield stress in Fig. 5.) Furthermore, it may be noted from Fig. 2 and Fig. 5 that the difference in inelastic buckling between Glare and pure aluminium plates is bigger for shear buckling. This is explained by the fact that, in shear loading, the fibres do not contribute to the shear stiffness of the Glare plate, which is due to the cross-ply arrangement of the fibres. This means that the shear load is almost entirely carried by the aluminium sheets, except for a small contribution from the resin material in the prepreg layers.

As an alternative, one could directly apply the “uniaxial” shear stress-strain curve of the Glare material to calculate the correction factor from Eq. (2) (and thereby neglecting the bending effects). The shear stress-strain curve of the aluminium layers is then represented by Eq.(11), from which the response of the entire laminate can be calculated when combined with the (elastic) glass properties. Results of this approach are presented in Fig. 6 for a RO parameter of $n = 10$, along with the solution from a CLT-based procedure where the shear secant modulus is used for the individual aluminium layers [13].

Contrary to the compression case, we see that the curve for the “uniaxial” approach differs only slightly from the curve for which the effect of bending is included (i.e. the CLT-based procedure) over the entire range. This is explained by the fact that the latter procedure explicitly calculates the correction factor as the ratio of the inelastic and elastic buckling stress. When in the plastic region, the stiffness moduli (i.e. E and G) of the aluminium sheets change according to the same ratio, $(G_s/G)_{al}$ [i.e. of the *aluminium* layers, calculated from Eq. (11)], so that the material remains more or less isotropic. Examining the bending stiffnesses (D_{11} , D_{22} , D_{12} , and D_{33}) of the bulk material in the plastic region, it shows that they all change in approximately equal ratios as well, especially in the early/moderately-plastic range where the aluminium is still dominating. It so turns out that the relative change in bending stiffness is similar to the relative change in secant modulus of the entire laminate, $(G_s/G)_{lam}$. Therefore, when applying Eq. (4) and assuming that the “ 4β -term” remains constant, a division of the plastic and elastic buckling stress gives a value not very different from $(G_s/G)_{lam}$.

It should be noted that the procedure of Ref. [13] uses the instantaneous value of Poisson’s ratio given by Eq. (14). When using the elastic value of Poisson’s ratio at all stress levels, the results of the CLT-based procedure and the “uniaxial G/G_s ” method almost overlap. In reality, the change in bending stiffness increases over the change in secant modulus when advancing in the plastic region, but the

“ 4β -term” in Eq. (4) actually decreases; therefore the laminated plate procedure produces a similar plasticity correction factor as Eq. (2).

Also shown in Fig. 6 is a curve corresponding to the J2-deformation theory approach proposed in the present work, and it can be seen that this method is more conservative than those employing the shear secant modulus. In the highly plastic region the results tend to converge to the same value for the correction factor, which should theoretically be the case since at these stress-levels the response is predominantly governed by the elastic fibre layers.

4 FEM analysis

To compare the plastic buckling results from the J2-deformation theory, a number of calculations were made with imperfect plates on the basis of J2-flow theory. For this purpose the STAGS [14] FEM code, which utilises an implementation of J2-flow theory according to the White-Besseling model, was used. Since the magnitude of the initial imperfection greatly affects the plate response, this particular phenomenon has been investigated as well.

4.1 Analysis procedure

The first step performed was always a linear bifurcation buckling analysis, in order to obtain the elastic critical load. This load was then used in the non-linear analysis to normalise the applied increments along the equilibrium path. The subsequent non-linear analyses can be divided into the following steps:

1. The critical bifurcation buckling load of the *perfect* plate is calculated following the elasto-plastic pre-buckling path. (This essentially yields bifurcation results on the basis of J2-flow theory). The main purpose is to determine the inelastic buckling *mode*, which may be different from the elastic one.
2. The buckling mode corresponding to the elasto-plastic critical load is imposed upon the plate geometry, serving as an initial imperfection. Non-linear plate response is

then calculated for different amplitudes of the imperfection.

The buckling analyses represented by Eqs. (3) and (4) are theoretically only valid for infinitely long plates. The plates used in the FEM calculations were taken with an aspect ratio of $a/b = 5$, which can be considered “sufficiently long”; for longer plates, the buckling load is virtually independent of the length. Moreover, the length effect is minimised by the fact that the plasticity correction factor is merely calculated as a ratio of two buckling loads—the elastic and inelastic one—which both contain the length effect. The FEM calculations were made with a RO-parameter of $n = 10$.

As an example, the FEM analysis of a Glare plate with a length of $a = 675$ mm and width of $b = 125$ mm will be described in detail, for both the compression (with Glare 3-7/6-0.4) and shear (with Glare 3-5/4-0.4) case. The plate was modelled with 50 elements in the long direction and 10 elements in the transverse direction. The STAGS 410 shell element was used here. All four edges were provided with simple-support conditions (i.e. rotationally unrestrained), while the in-plane displacements were unrestrained. Note that the in-plane conditions at the edges are unimportant in a bifurcation analysis, but do have a great influence on the post-buckling behaviour of the plate.

4.2 Compression loading

The linear buckling analysis gave a critical compressive stress of $\sigma_{cr} = 253.8$ MPa, whereas the analytical solution of Eq. (3) yields a value of $\sigma_{cr} = 252.5$ MPa, from which it is evident that the FEM result is very accurate. The critical buckling mode has five half-waves (see Fig. 7a), which is also according to theory. The bifurcation analysis using the elasto-plastic pre-buckling path gave a buckling load at 89% of the elastic solution. This means that the plasticity correction factor according to J2-flow theory is $\eta_c = 0.89$. The buckling pattern now has six half-waves—as can be seen in Fig. 7b—which is the result of a “change in anisotropy” during plastic deformation. The value of the

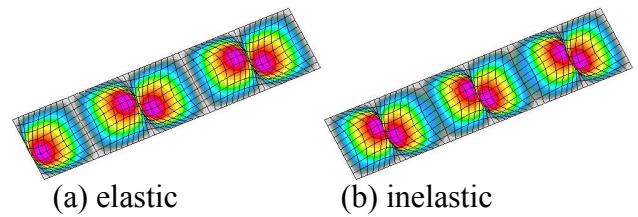


Fig. 7. Elastic and inelastic buckling modes of the example plate loaded in compression.

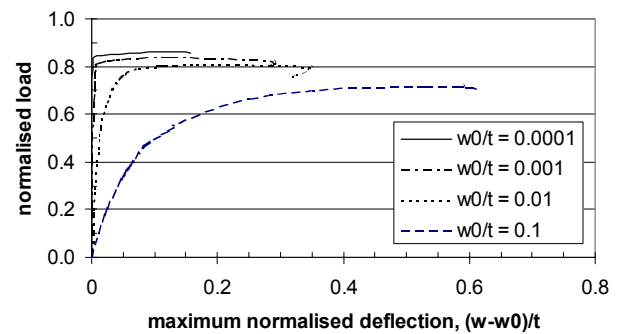


Fig. 8. Non-linear response curves for different imperfection magnitudes of the example plate loaded in compression.

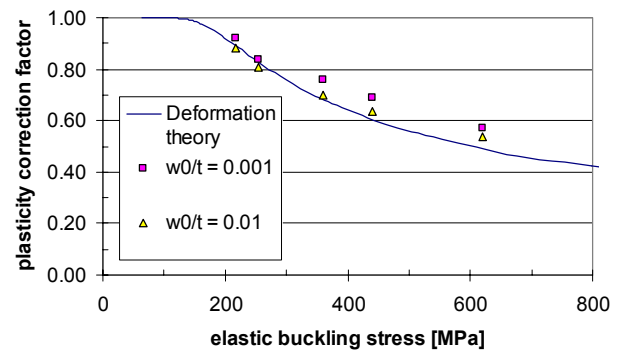


Fig. 9. Comparison of deformation theory and flow theory applied to compressed plates with different imperfection sizes.

correction factor for the calculation procedure discussed in this paper (i.e. based on deformation theory) is $\eta_c = 0.83$, which is about 7% lower than the value for flow theory.

The inelastic buckling pattern of six half-waves was used as an initial deviation from flatness of the plate, w_0 , for the subsequent non-linear analyses. Different amplitudes of this imperfection were considered; results for values of $w_0/t = 0.0001, 0.001, 0.01$, and 0.1 are plotted in Fig. 8, where the applied load is normalised with the elastic buckling load. The results show

that the imperfect plates exhibit limit point buckling behaviour (i.e. a maximum in the load-deflection curve), and that the magnitude of this limit point progressively decreases for growing initial imperfections. As the amplitude of the imperfection approaches zero, the value of the limit point moves towards the bifurcation load of the perfect plate for flow theory (previously calculated as 0.89). Taking the limit point as the critical buckling load, the correction factor for deformation theory ($\eta_c = 0.83$) lies between the results for imperfection sizes $w_0/t = 0.001$ ($\eta_c = 0.84$) and 0.01 ($\eta_c = 0.81$).

Results for Glare 3-7/6-0.4 plates of different widths are shown in Fig. 9 for two small imperfection sizes, $w_0/t = 0.001$ and 0.01. It can be seen that the buckling loads for imperfections of $w_0/t = 0.01$ agree generally well with the critical bifurcation loads of the deformation theory, but advancing in the plastic region, the deviation of the two different analysis methods increase.

4.3 Shear loading

The linear shear buckling stress of the Glare 3-5/4-0.4 example plate—with $a = 675$ mm and $b = 125$ mm—calculated with STAGS was found to be $\tau_{cr} = 181.4$ MPa. For a very long plate (i.e. $a \rightarrow \infty$, $b = 125$ mm), Eq. (4) yields a result of $\tau_{cr} = 173.0$ MPa, which is about 5% different from the FEM result. This discrepancy is higher than for the compression case, due to the higher complexity (e.g. skewedness) of the shear buckling deformation pattern, which is shown in Fig. 10. To reach the same accuracy as for compression, the shear model requires a (much) finer mesh density, which dramatically increases the computing time, in particular for a non-linear analysis. However, since the plasticity correction is calculated as the ratio of two buckling loads (which contain approximately the same error), this inaccuracy of 5% is irrelevant. The elasto-plastic bifurcation load on the basis of flow theory was calculated as 0.81 times the elastic one, so that $\eta_s = 0.81$. This value is considerably higher than $\eta_s = 0.69$, which is the result from the procedure based on deformation theory discussed in this

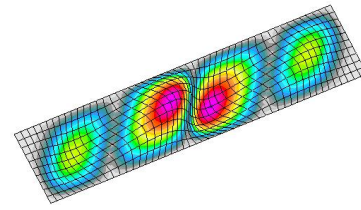


Fig. 10. Critical buckling mode of the example plate loaded in shear (same for elastic and inelastic case).

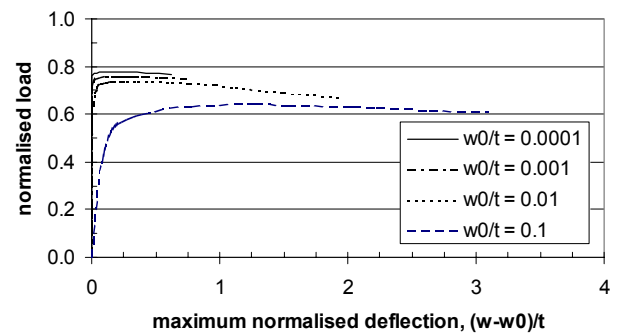


Fig. 11. Non-linear response curves for different imperfection magnitudes of the example plate loaded in shear.

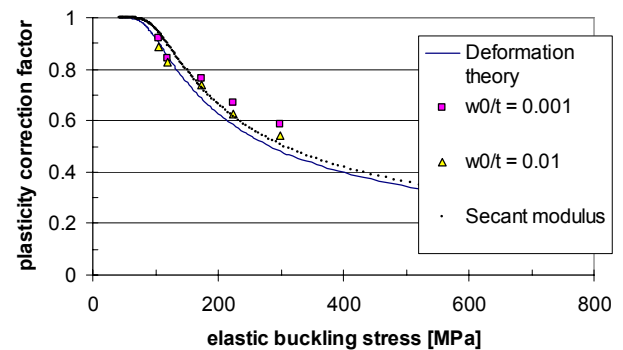


Fig. 12. Comparison of deformation theory and flow theory applied to plates loaded in shear with different imperfection sizes.

paper. The plastic buckling mode is the same as for the elastic case (shown in Fig. 10).

Analogous to the compressed plate (see Fig. 8), Fig. 11 presents load-deflection curves for the shear case for several amplitudes of the mode shape shown in Fig. 10, which is used as an initial imperfection in the non-linear analyses. The trends are the same as for the compression case, but it can be noted from the higher deflections that the plate loaded in shear was analysed further into the post-buckling region. It should be noted that in all cases—

including the compressed plates—the non-linear analysis was terminated by STAGS due to excessive plastic strains, which resulted in a singular stiffness matrix. In this case, the result for deformation theory (bifurcation buckling, perfect plate), $\eta_s = 0.69$, is bounded by the flow theory results (limit point buckling, imperfect plate) for imperfection sizes $w_0/t = 0.01$ ($\eta_s = 0.74$) and 0.1 ($\eta_s = 0.64$). Employing the shear secant modulus method of Ref. [13] (which corresponds to the “CLT-curve” in Fig. 6) a result of $\eta_s = 0.73$ is found, which is in better agreement with the flow theory predictions of $w_0/t = 0.01$ and 0.001 ($\eta_s = 0.76$).

Fig. 12 presents a comparison of buckling loads calculated with deformation theory analysis and STAGS results on the basis of flow theory, for Glare 3-5/4-0.4 plates. Also plotted is the curve according to the shear secant modulus method of Ref. [13]. It shows that in the early plastic region ($\eta_s = 0.80$ -1, say) there is a good agreement of the deformation theory and flow theory for small imperfections ($w_0/t = 0.001$ -0.01). For higher plastic buckling stresses, though, the shear secant modulus method correlates better with the STAGS results for imperfections of $w_0/t = 0.01$, but the difference tends to increase when advancing in the plastic region. However, for design purposes, use of the deformation theory seems favourable since it is the most conservative approach. It should be noted that in Fig. 12 the correction factors obtained from the FEM analyses are plotted against the *analytical* solution of the elastic shear buckling stress. In this way, the 5% error in elastic critical load is eliminated.

5 Discussion

The inelastic buckling behaviour of flat, rectangular Glare plates looks very similar for compression and shear loading, but the plasticity effect is more pronounced for the latter case. This is caused by two effects: for one, the shear yield stress of aluminium is lower than the direct yield stress and, secondly, the fibres are not stressed when the Glare plate is loaded in pure shear, so that virtually all the

load is carried by the aluminium layers. Obviously, to achieve a better performance in shear, the fibres should be aligned at ± 45 -degrees, in which case the fibres are fully utilised.

The results from the CLT-based procedure proposed in the present paper were also compared to the “classical” approach (i.e. for fully metallic plates) employing the uniaxial stress-strain curve of the Glare plate. For compressed plates, the results from both methods agree closely for buckling stresses up to 80% of the aluminium yield stress. This can be explained by the fact that the bending stiffness decreases more rapidly than the membrane stiffness when the aluminium becomes plastic, which is due to the stacking sequence (aluminium is at the outside of the laminate). In the advanced-plastic region, where the aluminium has become weak, the glass fibre layers govern the laminate response.

For shear, the “classical” reduction factor of Eq. (2), which utilises the shear stress-strain curve of the laminated plate, gives results that are almost equal to those from a procedure where the bending is explicitly included (Ref. [13]). The reason for this is that the latter procedure explicitly calculates the plasticity correction factor as the ratio of two buckling stresses. This ratio is mainly determined by the changes in plate bending stiffnesses, which are similar to the change in shear modulus, G_s/G , of the plate. Application of the deformation theory in conjunction with CLT gives the most conservative plastic shear buckling stresses, and is therefore—while no experimental data is available for Glare plates yet—recommended for design purposes.

Principally, the results presented in this paper are only valid for the specific Glare types considered, since the contributions of the metal and fibre parts to the laminate stiffnesses are different for each Glare configuration. In practice, however, the difference between Glare configurations of the same grade (i.e. 2, 3, or 4) is relatively limited; on the other hand, the influence of the strain hardening parameter, n , is very pronounced indeed.

Comparison of STAGS FEM calculations of plates containing initial imperfections and using J2-flow theory, with bifurcation buckling results of perfect plates on the basis of J2-deformation theory, revealed that similar results are obtainable for relatively small imperfections (typically 0.1 to 1 percent of the plate thickness). For both the compression and shear case the limit point was taken as the inelastic buckling load of the imperfect plates.

The logical next step in the investigation is to correlate the results obtained in this paper with experimental data, in order to verify the accuracy of the developed calculation procedure. A practical problem, however, is the difficulty to implement exactly simply-supported or clamped edge conditions of the plate, which is needed for comparison with the theoretical solutions.

For aluminium plates loaded in compression, the test method employed in Ref. [3] seems a practical one. The specimens are actually long, extruded tubes of square cross-section, where the walls are the actual plates being tested. Because these “plates” have all the same dimensions and material properties, they buckle at (approximately) the same point, thereby simulating nearly simply-supported conditions at the long edges. (Note that for sufficiently long plates the conditions at the short edges are not so relevant.) If this method is to be used for Glare plates, a special manufacturing process needs to be devised so that the four “plates” have exactly equal properties, since extrusion is obviously not possible for Glare.

For shear loading, a three-rail shear test set-up as applied by Gerard [5] can also be used for Glare plates. In this case, the long edges are clamped. (Again, the individual “plates” are long so that the influence of the short-edge conditions is limited). Alternatively, a picture frame may be used to apply a pure shear load to a Glare plate, in which case all the plate edges are clamped. When installing torsionally rigid stiffeners, the test plate can be divided into smaller ones where, again, all edges are

clamped or nearly clamped. In this manner, the same test fixture can be used to obtain various values of buckling loads or, in other words, a range of plasticity correction factors.

Finally, it should be noted that experimental data does exist for plastic buckling of stiffened Glare panels loaded in shear, and that good correlation was obtained with FEM simulations using STAGS [15]. Noting this fact, the results for imperfect plates using flow theory may tentatively be considered for verification-purposes as the “next best thing” to actual test results.

Acknowledgement

The research presented in this paper was sponsored by the Dutch Technology Foundation (STW).

References

- [1] Vlot, A and Gunnink, JW (eds.). *Fibre Metal Laminates – an introduction*. Kluwer Academic Publishers, Dordrecht (NL), 2001.
- [2] Verolme, K. *The development of a design tool for Fiber Metal Laminate compression panels*. Ph.D. thesis, Faculty of Aerospace Engineering, Delft University of Technology, 1995.
- [3] Pride, RA and Heimerl, GJ. *Plastic Buckling of Simply Supported Compressed Plates*. NACA TN 1817, National Committee for Aeronautics and Astronautics, April 1949.
- [4] Gerard, G and Becker, H. *Handbook of Structural Stability – Part I, Buckling of Flat Plates*. NACA TN 3781, National Committee for Aeronautics and Astronautics, July 1957.
- [5] Gerard, G. Critical Shear Stress of Plates above the Proportional Limit. *Journal of Applied Mechanics*, Vol. 15, No. 1, pp. 7-12, 1948.
- [6] Shrivastava, SC. Inelastic buckling of plates including shear effects. *Int. J. Solids Structures*, Vol. 15, pp. 567-575, 1979.
- [7] Hutchinson, JW. Plastic Buckling. *Advances in Applied Mechanics*, Vol. 14, pp. 67-144, 1974.
- [8] Anonymous. *Metallic Materials and Elements for Aerospace Vehicle Structures*. MIL-HDBK-5H, U. S. Government Printing Office, Washington, D.C., December 1998.
- [9] Anonymous. *Polymer Matrix Composites – Volume 2. Material Properties*. MIL-HDBK-17-2E, U. S. Government Printing Office, Washington, D.C., January 1997.
- [10] Ashton, JE and Whitney, JM. *Theory of Laminated Plates*. Technomic Publishing Co., Inc., Stamford

**PLASTICITY CORRECTION FACTORS FOR FLAT RECTANGULAR
GLARE PLATES LOADED IN COMPRESSION OR SHEAR**

(Conn., USA), 1970.

- [11] Peek, R and De Jonge, A. A plasticity theory to predict wrinkling of imperfect pipes. Paper presented at *Offshore Mechanics and Arctic Engineering Conference 1998 (OMAE 1998)*.
- [12] Needleman, A and Tvergaard, V. Necking of biaxially stretched elastic-plastic circular plates. *J. Mech. Phys. Solids*, Vol. 25, pp. 159-183, 1977.
- [13] Wittenberg, TC and Van Baten, TJ. Plastic Buckling Analysis of Flat Rectangular FML Plates Loaded in Shear. In *Proceedings of the 32nd International SAMPE Technical Conference*, Boston (MA., USA), pp. 673-686, November 2000.
- [14] Rankin, CC, Brogan, FA, Loden, WA, and Cabiness, HD. *STAGS Users Manual – Version 3.0*, Lockheed Martin Missiles & Space Co., Inc., December 1997.
- [15] Wittenberg, TC, Van Baten, TJ and De Boer, A. Design of FML shear panels for Ultra-High Capacity Aircraft. *Aircraft Design*, No. 4, pp. 99-113, 2001.